

Influence of coaxial cylinders on vortex breakdown in a closed flow.

Cecilia Cabeza^a, Gustavo Sarasúa^a, Arturo C. Martí^a, Italo

Bove^a, Sylvana Varela^{a,b}, Gabriel Usera^{b,c}, and Anton Vernet^b

^a*Instituto de Física, Universidad de la República, Montevideo, Uruguay*

^b*Departament d'Enginyeria Mecànica, Universitat Rovira i Virgili, Tarragona, Spain and*

^c*Instituto de Mecánica de los Fluidos, Facultad de Ingeniería,*

Universidad de la República, Montevideo, Uruguay

(Dated: November 15, 2018)

The effect of fixed cylindrical rods located at the centerline axis on vortex breakdown (VB) is studied experimentally and numerically. We find that the VB is enhanced for very small values of the rod radius d , while it is suppressed for values of d beyond a critical value. In order to characterize this effect, the critical Reynolds number for the appearance of vortex breakdown as a function of the radius of the fixed rods and the different aspect ratios was accurately determined, using digital particle image velocimetry. The numerical and experimental results are compared showing an excellent agreement. In addition, a simple model in order to show that this effect also appears in open pipe flows is presented in the appendix.

PACS numbers: 47.32.-y, 47.32.cd, 47.32.Ef

Keywords: vortex breakdown, recirculation flow, control

I. INTRODUCTION

The development of structural changes in vortical flows and, particularly, vortex breakdown [1, 2, 3, 4, 5] has been intensively investigated during the last years [6, 7, 8, 9, 10, 11, 12, 13, 14, 15, 16, 17, 18]. The characteristic and fundamental signature of vortex breakdown is the appearance of a stagnation point followed by regions of reversed axial flows with a bubble structure when the swirl is sufficiently large. This structural change is also accompanied by a sudden change of the size of the core and the appearance of disturbances downstream the enlargement of the core. Vortex breakdown is very important in several applications of Fluid Mechanics such as aerodynamics, combustion, nuclear fusion reactors or bioreactors. The presence of this phenomenon in these devices may be beneficial or detrimental, depending on each particular application [11, 13].

Vortex breakdown (VB) has been firstly observed in open flows [1], but subsequently it has been obtained also in experiments performed in confined flows, for example, in closed cylinders [3]. It is worth noting that the characteristics of VB in both cases are strongly similar, suggesting the possibility that the basic mechanism of VB is the same in both situations [10]. Experimental measurements show that flows in open channels can be accurately described with the relatively simple q-vortex model [5]. On the other hand, an analytical description for closed flows which are considerable more complex than closed flows is not known [3, 6, 7]. Thus, experiments performed with flows confined in cylinders are very attractive in order to understand the basic mechanism of VB, as well as investigate possible control mechanisms.

Due to the great number of practical implications of VB, the development of mechanisms for controlling its emergence is of considerable interest. Recently, different methods for controlling VB in closed flows have been proposed using different techniques. The effect of adding a small, rotating or stationary, cylinder was first investigated using numerical and experimental techniques, by Mullin *et al* [12]. Husain *et al* [11] considered the addition of co- or counter rotation near the axis using a small central rod rotating independently of the bottom or rotating end wall. They concluded that such method may be an effective way to either enhance or suppress VB. Other approaches are based on the introduction of a small rotating disk in the end wall opposite to the rotating wall [13, 19, 20], or the use of axial temperature gradients [21].

In the Ref. [12], the authors found that a straight small cylinder does not change qualitatively the characteristics of the flow. They also considered the case of a stationary cylinder for fixed aspect ratio and Reynolds number they did not find important qualitative changes with respect to the case without inner cylinder. They concluded that it is necessary to slope the inner boundary in order to significantly alter the VB bubble. However, as these authors recognize it is difficult to find a reliable measure for the onset of VB using dye visualization. It is clear that a more accurate technique is necessary in order to get quantitative experimental results for the VB onset.

The aim of this work is to analyze accurately the effect of the presence of a rod at the cylinder axis on the VB for an important range of parameters. Since the onset of VB is associated with the appearance of a stagnation point near the axis an accurate determination of the velocity field is necessary. Using the Digital Particle Image Velocimetry (DPIV) technique we obtain the critical Reynolds number for the onset of VB as a function of the aspect ratio and radius of the inner cylinder. In order to gain a deeper understanding of the internal structure of the flow and accuracy in

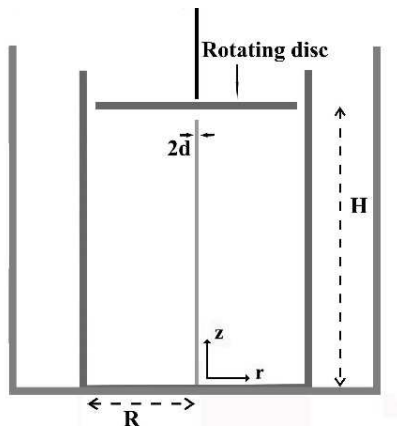


FIG. 1: The experimental setup consists of a closed cylinder, radius R and height H , with a rotating top wall. Along the axis of the cylinder a fixed rod of radius d is located. A external container was used in order to minimize the optical distortion of the images due to the curvature of the cylindrical wall.

the critical Reynolds numbers, we considered necessary to complement our experimental observations with numerical simulations. It is found that the existence of rods can affect significantly the critical value of the Reynolds number, Re_c for the onset of the VB.

This paper is organized as follows. In Sec. II we present the experimental setup and general observations. In section III, we describe the numerical method used in the simulations. The comparison between the experiments and the numerical calculations is given in Sec. IV. Finally, in Sec. V, we present a summary and the conclusions.

II. EXPERIMENTAL SETUP

The experimental setup consists of an plexiglas cylindrical container of inner radius $R = 40.0$ mm, a rotating disk at the top and a fixed disk at the bottom of the cylinder (see figure 1). The rotating disk is driven by an electronically controlled DC motor, operating between $\Omega = 1$ rad/s and $\Omega = 21$ rad/s, with an error of less than 0.5% in the measurement of Ω . The height H of the flow domain, and therefore the aspect ratio H/R , can be varied by moving the rotating disk up and down to a predetermined location. In this work, four different aspect ratios H/R : 1, 1.5, 2 and 2.5 were used.

In a first series of experiments, the emergence of vortex breakdown in absence of rod for comparison with results of previous works is studied. In the second part of the experimental work, the effect of axial rods on VB development is investigated. We use the cylinder described above, with an axial rod fixed on the bottom disk. The rod was perfectly aligned along the axis of the cylinder and was kept at rest during the experience. Three different rod sizes, with corresponding radius $d = 1.0$ mm, $d = 2.5$ mm and $d = 5.0$ mm were used.

The fluid used was water dissolutions of glycerin at 60% in mass, with $\nu = 1.0 \times 10^{-5}$ m²/s. Neutrally buoyant polyamide particles of 50×10^{-6} m diameter was seeding inside fluid in order to obtain the velocity profile. A vertical green laser sheet of 100 mW, with 2 mm of width was used as an illumination system. The sheet was focalized at the meridional plane of the cylinder. The images of the flow were record using a CCD camera at 90 fps. In order to minimize optical distortion of images due to the curvature of the cylinder in the onset of VB a stagnation point in the axis appears in the flow. In this case, the vertical velocity at the axis is null and we used this fact to

Figure 2 shows the typical DPIV images for the onset of VB corresponding to different radius of the rod. The container was immersed in a rectangular box filled with the same working fluid, since both the solution and the plexiglas have similar refractive indices. The experiments were conducted in an air-conditioned room at 20°C and the fluid temperature was monitored regularly using a thermocouple located at the bottom of the external container. The Reynolds number was defined as in previous studies as $Re = \Omega R^2 / \nu$, which varies in the experiments between 600 and 2900, with a 2% of error.

The conventional Digital Particle Velocimetry Velocity (DPIV) technique was implemented in order to obtain the velocity field inside the flow. This technique allow us to get accurate quantitative values of the velocity profile based on the cross-correlation of two consecutive images. In fact, this technique allow us to determine accurately the critical Reynolds number (Re_c) at the onset of VB through the measurement of the vertical velocity at the axis of the cylinder. The onset of VB is typically associated with localized regions of reverse flows, i.e. an internal stagnation point on the

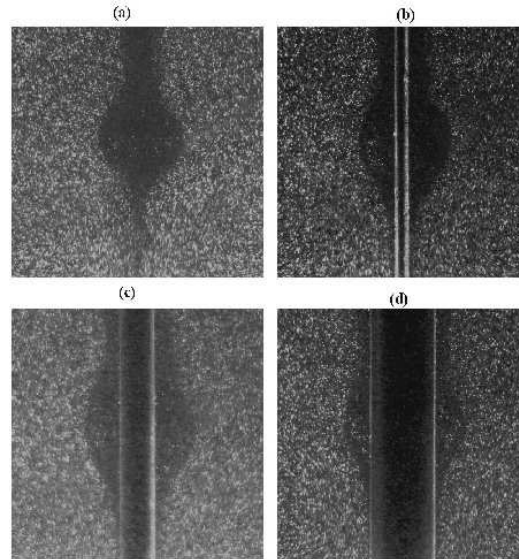


FIG. 2: Magnifications of the zone corresponding to the recirculation bubble at the onset of VB for different radius of the rod. The aspect ratio ($H/R = 2$) is the same in all the images while the Re_c varies in each image: (a) $Re = 1474$, without rod. (b) $Re = 1313$, $d = 1.0\text{mm}$, (c) $Re = 1431$, $d = 2.5\text{mm}$. (d) $Re = 1671$, $d = 5.0\text{mm}$.

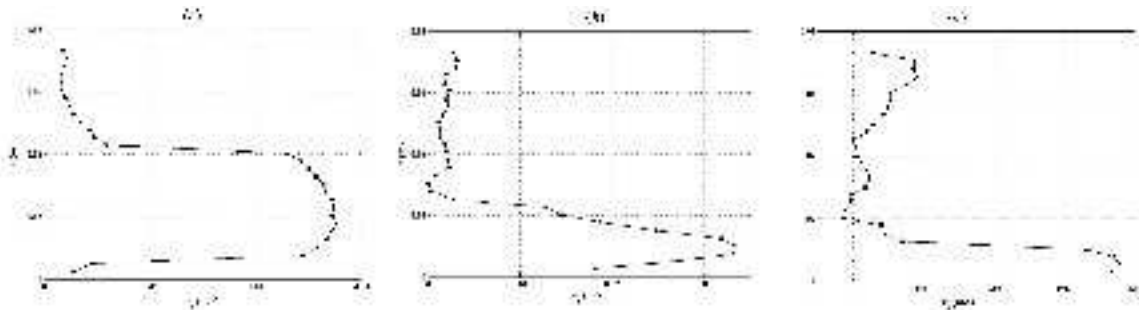


FIG. 3: Axial velocity profiles at the axis ($r = 0$) for $H/R = 2$ obtained using the DPIV technique and corresponding to the cylinder without rod. (a) situation before the onset of VB, $Re = 1391$, the axial velocity at the axis is always positive. (b) first VB, $Re = 1474$, the axial velocity at the axis present a null value at the stagnation point located at $z_c = 3.1$ cm. (c) onset of the second VB, $Re = 1836$, in this case the axial velocity at the axis presents a range of negative values in the place of the first recirculation bubble and a second stagnation point at $z_c = 4.5$ cm where the second bubble is going to appear.

vortex axis appears, located at a certain height, (z_c). The appearance of VB bubbles is a manifestation of internal separation of the streamlines from the axis, causing the reversal of the axial velocity. We used the criteria that VB arises when the axial velocity changes the sign at the axis. In the situation when a fixed rod is localize at the axis of the cylinder, we analyze the vertical velocity at the wall of the rod.

Figure 2 shows the typical DPIV images for the onset of VB corresponding to different rod radius.

In figure 3 three typical axial velocity profiles at the axis ($r = 0$) for $H/R = 2$ correspondig to the cylinder whitout rod are show. In Fig. 3 (a) previous to the onset of VB the axial velocity is always positive and in this case the Reynold number is $Re = 1391$. At the onset of VB, Fig. 3 (b) corresponding to $Re_c = 1474$, the axial velocity present a null value at the stagnation point located at $z_c = 3.1$ cm above the bottom of the cylinder. Finally, in Fig. 3 (c) we can observe that the second VB take place at $Re_c = 1836$. In this case the axial velocity at the axis presents a range of negative values in the place of the first recirculation bubble and a second stagnation point at $z_c = 4.5$ cm above the bottom of the cylinder.

III. NUMERICAL METHOD

The numerical simulations considered here were obtained with the in-house flow solver `caffa3d.MB` developed jointly by Universitat Rovira i Virgili (Tarragona, Spain) and Universidad de la República (Montevideo, Uruguay). It is an original Fortran95 implementation of a fully implicit finite volume method for solving the 3D incompressible Navier-Stokes equations in complex geometry, using block structured body fitted grids. This three-dimensional solver is based on a two-dimensional solver described in [24]. Further description of this model can be found in Ref. [25, 26].

The mathematical model comprises the mass (1) and momentum (2) balance equations for an incompressible Newtonian fluid:

$$\int_S (\vec{v} \cdot \hat{n}_S) dS = 0 \quad (1)$$

$$\int_{\Omega} \rho \frac{\partial u}{\partial t} d\Omega + \int_S \rho u (\vec{v} \cdot \hat{n}_S) dS = \int_S -p \hat{n}_S \cdot \hat{e}_1 dS + \int_S (2\mu \mathbf{D} \cdot \hat{n}_S) \cdot \hat{e}_1 dS \quad (2)$$

These equations hold in any portion Ω of the domain, being S the boundary of Ω and \hat{n}_S the outward normal vector at the boundary S . The momentum balance equation (2) has been expressed for the first component u of the velocity vector $\vec{v} = (u, v, w)$, with similar expressions holding for the other components. The viscosity μ of the fluid and the symmetric deformation tensor \mathbf{D} were used for the viscous term.

Since the Reynolds number was relatively low for all cases, since $Re = 800$ to $Re = 2700$, no turbulence model was required so transient solutions were computed directly. The time step was set to 10^{-1} s for all cases. Simulations were run starting from null velocity fields through 10^3 time steps, or about 100 s of flow time.

Two different grids were used, one to study the fluid without rods, and other to study the system including the rods. To study the system with rod C-grid block, with a no-slip boundary condition at walls, Fig. 4(b), is used. The different choice of grid topology for the two cases reflects that a boundary condition near the axis exists for the case that includes rods, while no boundary condition exists at the axis for the case without rods. Thus, the two-block grid strategy adopted for the second case ensures that the critical region near the axis is treated entirely as an inner region in the absence of a rod, not requiring the specification of delicate boundary conditions there. On the other hand, for the case that includes rods, the single cylindrical block is the natural choice allowing a direct specification of the non-slip boundary condition at the rod. On the other hand, the grid used for the cylinder without rods is a block structured grid, made of two blocks. The inner one is a prism of a square base of 5 mm (0.2592×10^6 cells) located in the axis of the cylinder, while the outer one is a C-grid block that wraps around the first one, see Fig. 4 (a) (2.304×10^6 cells).

The numerical model allows us to get the three components of the velocity field (v_r , v_θ , v_z) and its derivatives. As mentioned before, the reversals of the axial component of the velocity v_z in the region near the axis gives us information on the emergence of areas of recirculation (bubbles), which are a way of determining VB. In Fig. 5 numerical results of the axial component of the velocity are showed for the cylinder without rod. The two showed panels correspond to one (top) and two (bottom) VB bubbles. This velocity profiles show an excellent agreement with those obtained experimentally (Fig. 3).

The simulations are performed for different cases (three values of the aspect ratio H/R , cylinder with and without rods) and Reynolds numbers. The numerical results are in excellent agreement with the experimental velocity profiles. The position of the stagnation point is obtained with a difference less than 5% in the system with and without rods. The numerical results were analyzed through streamlines ψ and azimuthal vorticity $\eta_\theta = \eta_y \cos \theta - \eta_x \sin \theta$. In addition, the energy density, defined as $e = \frac{p}{\rho} + \frac{1}{2}(v_r^2 + v_\theta^2 + v_z^2)$, the velocity module and the pressure field were obtained (not shown in this work).

Figure 6 shows contours for the azimuthal vorticity η_θ in the meridional plane for $H/R = 2$ at critical Reynolds number Re_c as indicated. The contour levels are non-uniformly spaced, with 20 levels in the positive range and 20 in the negative one determined by $level_{pos}(i) = Max(variable) \times (\frac{i}{20})^3$ and $level_{neg}(i) = Min(variable) \times (\frac{i}{20})^3$ [6]. All are plotted at $t = 100$ s, when steady-state flow conditions have been reached.

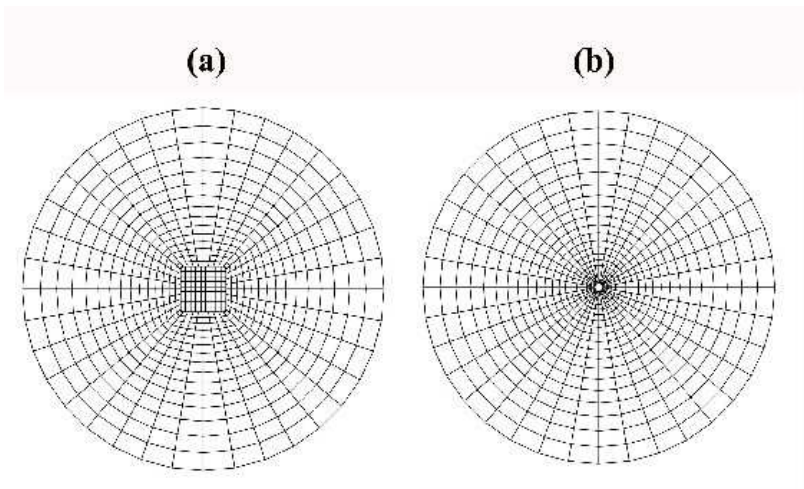


FIG. 4: (a) Cross section of the block-structured grid, with a central square block, used in the case of the cylinder without rod. This grid topology prevents the need for internal boundary conditions at the axis of the domain for the case without rod. (b) Cross section of the structured grid for the case of the cylinder with rod.

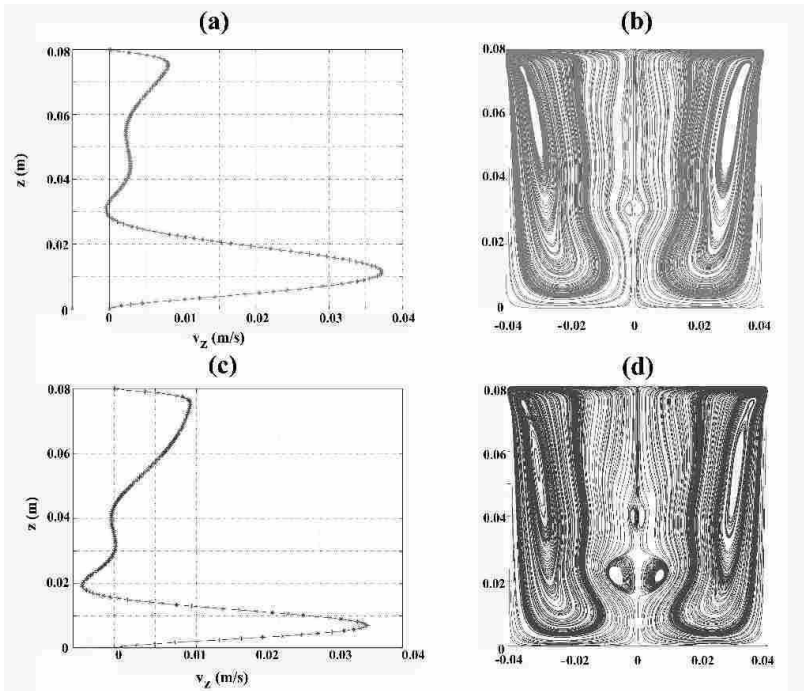


FIG. 5: Numerical results of the axial velocity profiles (left) and streamlines (right) corresponding to the same situation of figure 3. (a) and (b) one bubble is observed for $H/R = 2$ and $Re = 1474$. (c) and (d) two bubbles are observed for $H/R = 2$ and $Re = 1836$.

IV. RESULTS AND DISCUSSION

For convenient comparison with previous works [3], we first studied the emergence of vortex breakdown in absence of rods. In table IV the experimental and numerical results for the onset of VB for different aspect ratios are shown. In this table also Escudier results are shown. First, if we compare our experimental and numerical results, we can observe that its present an excellent agreement with a difference lower than 2%. In second place, our results are in very good agreement with the results of Escudier [3]. Our results present a difference lower than 3% respect to

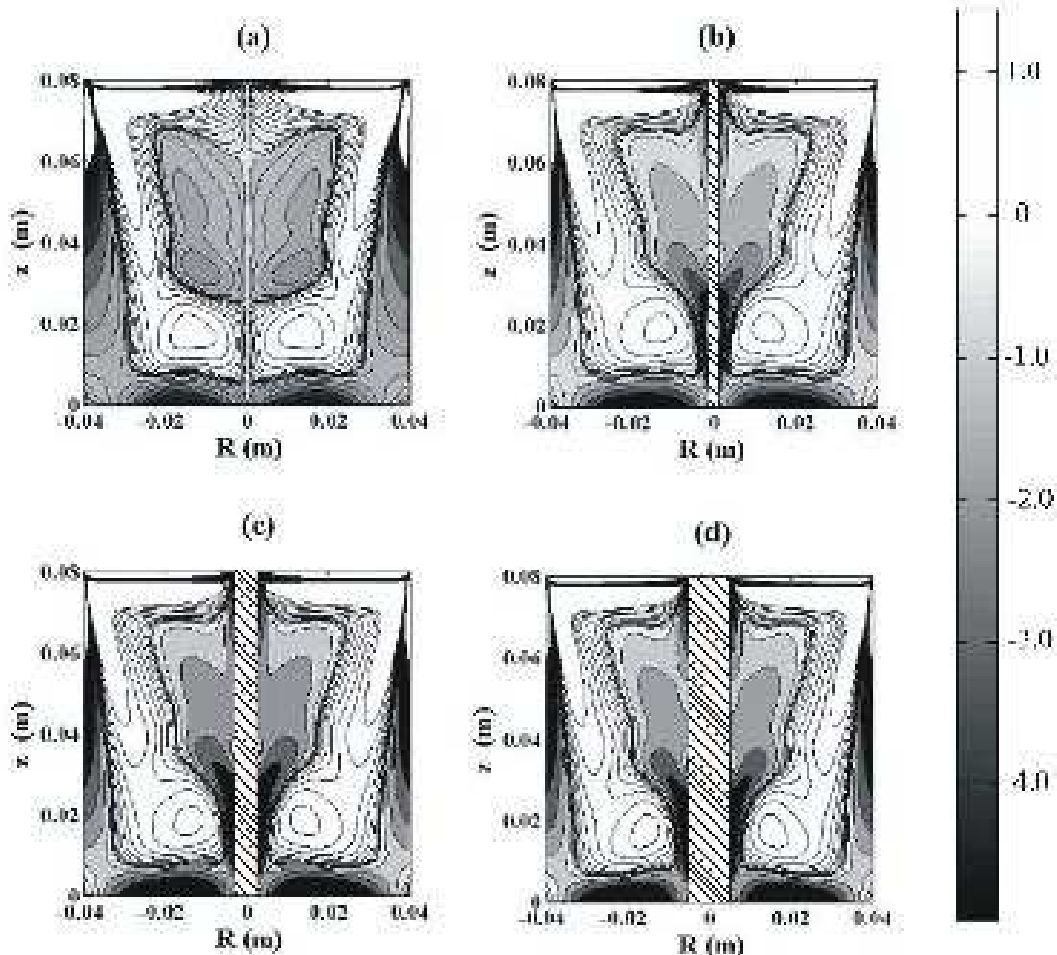


FIG. 6: Numerical results for the azimuthal component of the vorticity at the onset of VB and aspect ratio $H/R = 2$. The lined regions represent the fixed rod. (a) without rod, $Re = 1474$, (b) fixed rod of radius $d = 1.0$ mm and $Re = 1340$. (c) fixed rod of radius $d = 2.5$ mm and $Re = 1435$. (d) fixed rod of radius $d = 5.0$ mm and $Re = 1700$. The scale, indicated in the colorbar at the right, is the same for all the panels.

Escudier's results. We can conclude that the method experimental and numerical that we have used are very reliable. Thus, the DPIV technique provide an accuracy method to determinate the onset of the VB through the analyze of vertical velocity profile. The result presents in this work shown that the DPIV technique are more realible that one based in visualization using dye technique.

Now, we consider the situation in which an axial fixed rod of radius d is present. In table IV for $d/R = 0.025$ we can observe that the Reynolds number necessary to achive the onset of VB is less than the case without fixed rod. Meanwhile for $d/R = 0.0625$ the onset is achived for Re_c slightly lower than $d/R = 0$ and for $d/R = 0.1250$ the Re_c present values 15% above than the case without rod.

In figure Fig 7 is depicted a comparison between the experimental and numerical results concerning the effect of the cylinders on the first bubble formation, showing that there is a very good agreement. We show the Re_c as function d/R for the three aspect ratio that we have studied. In order to analyze the response of the system when the radius of rod is increased, we calculated numerically the Re_c for $d/R = 0.25$. The difference in the Reynolds number at the onset is approximately 65% between cylinder without and with rod, for all aspect ratio analyzed here. In summary, we can conclude that if the aspect ratio is kept constant, increased the radius of the rod represent a significative

H/R	d/R=0			d/R=0.0250		d/R=0.0625		d/R=0.1250	
	Exp. (1)	Exp. (2)	Num.	Exp. (2)	Num.	Exp. (2)	Num.	Exp. (2)	Num.
1.5	1068	1098	1095	971	950	1036	1020	1246	1200
2	1450	1474	1474	1313	1340	1431	1435	1671	1700
2.5	1910	1973	1935	1785	1780	1887	1910	2187	2250

TABLE I: Experimental and numerical critical Reynolds numbers corresponding to the appearance of the first VB for different aspect ratios and radius of the rod. The experimental values (1) were taken from [3] and the (2) were obtained in this work using the DPIV technique.

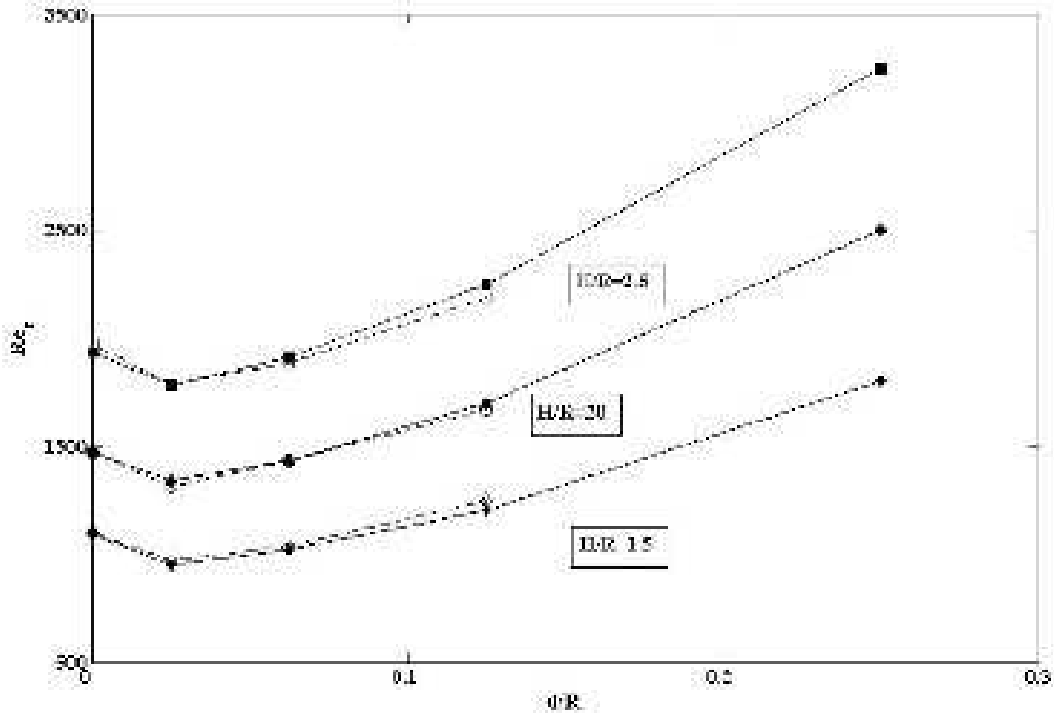


FIG. 7: Experimental (open symbols) and numerical (filled symbols) values of the critical Reynolds numbers corresponding to the appearance of the first bubble as a function of the rod radius, for different values of the aspect ratio $H/R = 1.5$ (diamonds), $H/R = 2.0$ (circles) and $H/R = 2.5$ (squares)

change in the Re_c at the onset and for small radius of the rod, the Re_c is lower than the case without rod. However, there is a region of radius of the rod, that depend of aspect ratio, which slightly variation is observed for the Re_c between cylinder with and without rod.

A clear modification is noted also in the vorticity structure, as can be seen from Fig. 6. For $d = 2.5$ mm and $d = 5.0$ mm, we observe that the critical Reynolds number to begin vortex breakdown is increased. The effect in the structure of the vorticity in these cases are similar to the observed for the smallest rod. Experimental and numerical for the critical value Re_c are summarized in Table IV.

It is interesting to compare our results with those obtained in references [12], [11]. In these two works, it was concluded that a very slender rod at rest does not introduce significant changes in VB phenomena. The radius ratio used by these authors was $d/R = 0.04$, which is similar to the small radius ratio value we considered, that is $d/R = 0.025$. In reference [12], the authors used an inner cylinder with ratio $d/R = 0.1$. In our experiments we observed appreciable changes in the critical value of Re, for all values of the ratios considered. Looking carefully at Figures 2 and 3 of [12], we observe slight differences which, according to the authors, are within the experimental errors. For this reason, we took specially careful measurements in these cases.

At this point it is interesting to consider the origin of the effect of the rod on VB, and in particular if it is of viscous nature or not. Inviscid theory has largely used to explain the origin of VB. The results has been sufficiently succesfull to support the belief that VB may occur with no presence of viscosity. In ref. [7], Brown and Lopez argued that VB in closed flows takes place in conditions for which the flow may be considered as inviscid. In this case, a change of sign in the azimuthal component of vorticity η_θ is expected to occurs near the stagnation point [7]. This condition is verified in the VB that takes place without rod, as can be seen in figure 6a . In this figure, the stagnation point occur at $z = 0.032$, where z measures the height from below. However, this condition is not satisfied in the presence of the rods. In these cases, the stagnation point occur near $z = 0.03$ on rod surface. This point is surrounded with a region of constant η_θ sign, as can be seen in figures 6b,c,d. Thus the relation of Brown and Lopez does not holds, showing that we cannot expect to describe the VB appropriately with only inviscid theory in the presence of rods.

The decrease of Re_c due to small rods appears to be of viscous origin. The presence of the rods tends to reduce the velocity of the fluid due to stress at the rod surface, favoring the appearance of the stagnation point and thus reducing the critical value Re_c needed for the appearance of VB. The reducing effect of the viscosity is also present in the absence of rods and may begin the process that leads to the formation of the stagnation point (as occur in pipe flows [7]), but the presence of the rigid limit imposed by the rod enhances this effect very much. Thus, a very thin rod produces an significative effect, because the boundary conditions at the axis changes drastically from free to no-slip. This produces an appreciable change in Re_c . A similar result was obtained in previous works where it has been shown that even though a thin wire may promote the formation VB in delta wings [22]. On the other hand, we note that when the diameter d is sufficiently large, the critical value of Re increases with increasing d (see Fig. 7). This effect is probably of inviscid origin. We support this conjecture with the results of a simple model for flows in a pipe, described in the appendix. With this model we obtain that the suppressing effect of increasing d also appears in unconfined pipe flows. Then, when d increases, this effect of inviscid nature compensates the viscous one and finally the VB is displaced to higher values of Re .

V. SUMMARY AND CONCLUSIONS

In this work, we studied the changes in the VB phenomena that are produced when a rod is located at the axis of the cylinder container i.e. the vortex centerline. The experiments shown that the rod may increase or decrease the critical Reynolds number for the emergence of VB. The effect of small rods is to decrease Re_c , while Re_c is increased when d/R is beyond a certain critical value $(d/R)_c$, which is of order 0.06. This critical value depends weakly on the aspect ratio, decreasing smoothly with increasing H/R . The effects of the rods of practical interest since may be used to perform a control of the VB in a way that is simpler than other previously proposed in the literature, since it does not require additional auxiliary devices. It is worth noting that this method, unlike the approach proposed in previous works, does not imply the addition of swirl near the axis. This simplicity is an interesting feature, making it more feasible to be used in engineering devices. The modification of the critical Re are very noticeable. The volume ratio (cylinder to row) is $V_1/V_2 \sim 4 \times 10^{-3}$, while the decrease of the critical Reynolds number is about 10% . So that the shift of the critical Reynolds number is 20 times larger that the percent modification of the volume of the cylinder, showing the effectiveness of the method. The dependence of the critical Re with the rod diameter obtained experimentally is in very good agreement with the found with numerical calculations. Using a simple theoretical model for flow in pipes, we obtained that the influence of the inner cylinder on the VB works in similar fashion in open flows, mainly for not too small values of $(d/R)_c$. We gave arguments to support that the enhancing effect of very small rods on VB is of viscous origin.

We acknowledge financial support from the Programa de Desarrollo de Ciencias Básicas (PEDECIBA, Uruguay) and Grants FCE 9028 and PDT54/037 (Conicyt, Uruguay).

APPENDIX

In this appendix, we consider a model for VB in open swirling pipe flows. Our interest is to study how the VB is affected when an inner cylinder is located at the axis of the duct. With this purpose, we use a simple model based on the failure of the cylindrical solution. In the past, it has been shown that simple theoretical vortex models of open flows may predict with some accuracy the emergence of vortex breakdown. A classical approach based on axisymmetric inviscid analysis was given by Batchelor [23]. In this model, it is assumed that initially the fluid moves inside a cylindrical duct of radius a_1 , with a Rankine vortex velocity field, and goes to another duct limited by two cylindrical boundaries of different radius. When the flow develops the stagnation point, the radial component of the velocity becomes important and the cylindrical approximation is no longer valid [4]. This is reflected in the disappearance of cylindrical solutions. Thus in this model, the disappearance of cylindrical solutions is identified with the emergence of VB [23].

In a cylindrical system of coordinates (r, θ, z) the velocity field of the assumed upstream flow is written as:

$$v_r = 0, \quad (3)$$

$$v_\theta = \begin{cases} \sigma r & 0 < r < a_2, \\ \Gamma/r & a_2 < r < a_1, \end{cases} \quad (4)$$

$$v_z = U_0. \quad (5)$$

where σ, Γ and U_0 are constants, with $\Gamma = \sigma a_2^2$, in order to impose the continuity of the velocity. We introduce the streamfunction Ψ defined as

$$v_z = \frac{1}{r} \frac{\partial \Psi}{\partial r}, \quad v_r = -\frac{1}{r} \frac{\partial \Psi}{\partial z}. \quad (6)$$

Employing the momentum conservation we obtain the following equation for the streamfunction:

$$r \frac{\partial}{\partial r} \left(\frac{1}{r} \frac{\partial \Psi}{\partial r} \right) + \frac{\partial^2 \Psi}{\partial z^2} = r^2 \frac{de}{d\Psi} - K \frac{dK}{d\Psi} \quad (7)$$

where $e = \frac{1}{2}v^2 + \frac{p}{\rho}$ and $K = rv_\theta$. For the flow given by Eqs. (3), we have that

$$e = \frac{2\sigma^2}{U_0} \Psi + \frac{1}{2}U_0^2, \quad K = \frac{2\sigma}{U_0} \Psi, \quad \text{for } 0 < r < a_1 \quad (8)$$

The same relations hold downstream for the steady flow, and so that Eq. (7) takes the form for the rotational part, if we restrict ourselves to consider cylindrical solutions,

$$\Psi(r) = \frac{1}{2}U_0 r^2 + AF_1(\gamma r) + BY_1(\gamma r) \quad (9)$$

where F_1 and Y_1 are the Bessel functions of the first and second kind respectively and $\gamma = 2\sigma/U_0$ [23]. The irrotational part of the flow is given by $v_\theta = \Gamma/r$, $v_z = U$, $v_r = 0$.

We particularize now to consider the situation in which the upstream flow goes two a duct limited by two cylindrical surfaces of inner radius d and outer radius R . The unknown constants which appear in Eq. (9) can be determined imposing the mass conservation and the continuity of the pressure. From these conditions, we obtain the following equation that gives the value of the radius of the rotational core in the downstream duct c

$$\frac{(a_1^2 - a_2^2)}{(R^2 - b^2)} - \frac{A_{II}}{U_0} \gamma J_0(\gamma b) - \frac{B_{II}}{U_0} \gamma Y_0(\gamma c) - 1 = 0, \quad (10)$$

with

$$A_{II} = \frac{U_0}{2cd} \left[\frac{d(a_2^2 - c^2)Y_1(\gamma d) + cd^2 Y_1(\gamma b)}{J_1(\gamma c)Y_1(\gamma d) - J_1(\gamma d)Y_1(\gamma c)} \right], \quad (11)$$

$$B_{II} = \frac{U_0}{2cd} \left[\frac{d(a_2^2 - c^2)J_1(\gamma d) + cd^2 J_1(\gamma b)}{Y_1(\gamma c)J_1(\gamma d) - Y_1(\gamma d)J_1(\gamma c)} \right]. \quad (12)$$

In figures 8 and 9 it is shown the value of c as a function of the nondimensional swirl parameter S , defined as $S = \gamma R$. From these figures we can see that at certain critical values S_c of S , two branches of solutions collide and disappear. According to the failure of the cylindrical approximation criteria, this is the value of S for which VB takes place. From these figures, we can see that the effect of a very slender inner cylinder may be to increase or diminish slightly the critical value S_c (the first case is observed in figure 8 and the second in figure 9). However, for all the situations considered, S_c increases with d , as long d is above a threshold. In this case, the emergence of VB was transferred to higher values of the nondimensional swirl parameter S and the VB was suppressed in the range of S values contained between the old and new critical values of S_c . These results shows that the present inviscid model predicts the suppressing effect of the slender cylinders, in analogy with the experimental observations of the closed

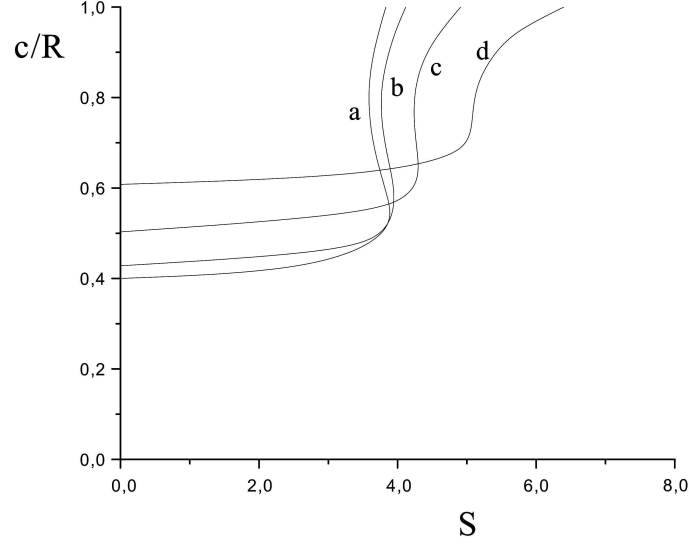


FIG. 8: Dimensionless core size, c/R , as a function of the swirl, S , for different radius of the fixed rod, (a) $d = 0$, (b) $d = 0.2$, (c) $d = 0.4$, (d) $d = 0.6$ and (e) , $d = 0.8$. Other parameter values: $R_0 = 1$, $c_0 = 0.4$ and $R = 1.2$

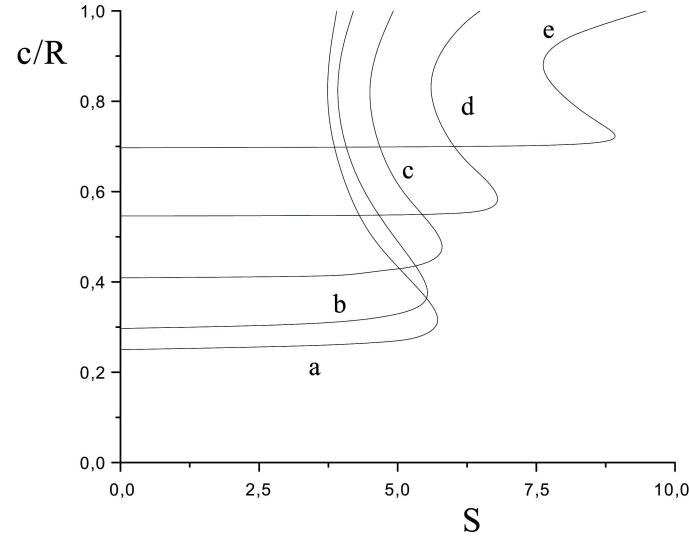


FIG. 9: As figure 8 but with $R_0 = 1$, $c_0 = 0.25$ and $R = 1.2$, for (a) $d = 0$, (b) $d = 0.2$, (c) $d = 0.4$, (d) $d = 0.6$.

flow, showing that viscosity is not necessary to explain this behavior. However, the decreasing effect on S_c that is observed for small values of d in figure 9, has nothing to do with the observed in the closed flow for the smallest of value of d , where the effect appears to be of viscous origin.

-
- [1] D. H. Peckham and S. A. Atkinson, "Preliminary results of low speed wind tunnel tests on a gothic ratio 1.0", Aeronautical Research Council Report CP 508, 1957.
 - [2] H.U. Vogel, "Experimentelle Ergebnisse ber die laminare Strmung in einem zylindrischen Gehuse mit darin rotierender Scheibe," MPI Bericht **6**, 1968.
 - [3] M. P. Escudier, "Observations of the flow produced in a cylindrical container by a rotating endwall," *Exp. Fluids* **2**, 189 (1984).
 - [4] S. Leibovich, "The structure of vortex breakdown" *Annu. Rev. Fluid Mech.* **10**, 221 (1978).
 - [5] S. Leibovich, "Vortex stability and breakdown: Survey and extension," *AIAA J.* **22**, 1192 (1984).
 - [6] J. M. Lopez, "Axisymmetric vortex breakdown. Part 1. Confined swirling flow," *J. Fluid Mech.* **221**, 533 (1990).
 - [7] G. L. Brown and J. M. Lopez, "Axisymmetric vortex breakdown. Part 2. Physical mechanisms," *J. Fluid Mech.* **221**, 553 (1990).
 - [8] J.M. López, "Unsteady swirling flow in an enclosed cylinder with reflectional symmetry," *Phys. Fluids* **7**, 2700 (1995).
 - [9] J.M. López, "Flow between a stationary and a rotating disk shrouded by a co-rotating cylinder," *Phys. Fluids* **8**, 2605 (1996).
 - [10] Mark C. Thompson and K. Hourigan, "The sensitivity of steady vortex breakdown bubbles in confined cylinder flows rotating lid misalignment", *J. Fluid Mech.* **496**, 129 (2003).
 - [11] Hyder S. Husain, Vladimir Shtern, and Fazie Hussain "Control of vortex breakdown by addition of near-axis swirl," *Phys. Fluids* **15**, 271 (2003).
 - [12] T. Mulin, J. S. Tavener, K. A. Cliffe, "On the creation of stagnation points near straight and sloped walls," *Phys. Fluids* **12**, 425 (2000).
 - [13] L. Mununga, K. Hourigan, and M. C. Thompson, "Confined flow vortex breakdown control using a small rotating disk," *Phys. Fluids* **16**, 4750 (2004).
 - [14] K. Fujimura, H. S. Koyama, J. M. Hyun, "A experimental study on vortex breakdown in a differentially-rotating cylindrical container," *Exp. Fluids* **36**, 399 (2004).
 - [15] M. Piva and E. Meiburg, "Steady axisymmetric flow in a open cylinder with a partially rotating bottom wall," *Phys. Fluids* **17**, 063603 (2005).
 - [16] A. Mitchell and J. Delery, "Research into vortex breakdown control," *Progr. Aerospace Sci.* **37**, 385 (2001).
 - [17] T.T. Lim and Y.D. Cui, "On the generation of spiral-type vortex breakdown in an enclosed cylindrical container," *Phys. Fluids* **17**, 044105 (2005).
 - [18] Z. Zhang and R. J. Hugo, "Stereo particle image velocimetry applied to vortex breakdown," *Exp. Fluids* **40**, 333 (2006).
 - [19] Peng Yu, Thong See Lee, Yan Zeng, and Hong Tong Low, "Effects of conoidal lids on vortex breakdown in an enclosed cylindrical chamber," *Phys. Fluids* **18**, 117101 (2007).
 - [20] P. Yu, T.S. Lee, Y. Zeng, and H.T. Low, "Characterization of flow behavior in an enclosed cylinder with a partially rotating end wall," *Phys. Fluids* **19**, 057104 (2007).
 - [21] M. A. Herrada and V. Shtern, "Vortex breakdown control by adding near-axis swirl and temperature gradients," *Phys. Rev. E* **68**, 041202 (2003).
 - [22] H. Akilli , B. Sahin and D. Rockwell, "Control of vortex breakdown by a coaxial wire", *Phys. Fluids* **15**, 123 (2003).
 - [23] G. K. Batchelor, "An introduction to Fluid Dynamics" (Cambridge University Press, Cambridge, 1967).
 - [24] Ferziger J. Peric M, "Computational methods for fluid dynamics", Springer-Verlag, (2002).
 - [25] G. Usera, A. Vernet, J. Pallares and J.A. Ferré, "A conditional sampling method based on fuzzy clustering for the analysis of large-scale dynamics in turbulent flows," *Eur. J. Mech. B Fluids* **25**, 172 (2006), G. Usera, A. Vernet, and J.A. Ferré, "A Parallel Block-Structured Finite Volume Method for Flows in Complex Geometry with Sliding Interfaces," *Flow. Turb. Comb.*, **80**, (2008).
 - [26] The code is freely available for academic use through the web site www.fing.edu.uy/imfia/caffa3d.MB